THE AMERICAN SOCIETY OF MECHANICAL ENGINEERS
345 E. 47th St., New York, N.Y. 10017

97-GT-162

HEAT TRANSFER PREDICTIONS FOR ROTATING U-SHAPED COOLANT CHANNELS WITH SKEWED RIBS AND WITH SMOOTH WALLS

Bernhard Bonhoff
Uwe Tomm
Bruce V. Johnson
ABB Corporate Research
CH5405 Baden-Dättwil
Switzerland

Ian Jennions
ABB Power Generation
CH5400 Baden
Switzerland

ABSTRACT

A computational study was performed for the flow and heat transfer in rotating coolant passages with two legs connected with a U - bend. The dimensionless flow conditions and the rotational speed were typical of those in the internal cooling passages of turbine blades. The calculations were performed for two geometries and flow conditions for which experimental heat transfer data were obtained under the NASA HOST project. The first model had smooth surfaces on all walls. The second model had opposing ribs staggered and angled at 45 deg. to the main flow direction on two walls of the legs, corresponding to the coolant passage surfaces adjacent to the pressure and suction surfaces of a turbine airfoil. Results from these calculations were compared with the previous measurements as well as with previous calculations for the nonrotating models at a Reynolds number of 25,000 and a rotation number of 0.24. At these conditions, the predicted heat transfer is known to be strongly influenced by the turbulence and wall models. The differential Reynolds-stress model (RSM) was used for the calculation. Local heat transfer results are presented as well as results averaged over wall segments. The averaged heat transfer predictions were close to the experimental results in the first leg of the channel, while the heat transfer in the second leg was overestimated by RSM. The flow field results showed a large amount of secondary flow in the channels with rotational velocities as large as 90 percent of the mean value. These secondary flows were attributed to the buoyancy effects, the Coriolis forces, the curvature of the bend and the orientation of the skewed ribs. Details of the flow field are discussed. Both the magnitude and the change of the heat transfer were captured well with the calculations for the rotating cases.

NOMENCLATURE

A	Van Driest constant (=0.26)
A-in,..,J-in	cross sections at the inlet of section A,..,J
c_p	specific heat of fluid
d_H	hydraulic diameter
E	wall function constant (=9.793)
e	rib height
k	turbulence energy
$\dot{m}$	coolant flow rate
Nu, Nu_∞	Nusselt number
p, Δp	pressure
Pr, Pr_t	laminar, turbulent Prandtl numbers
P	rib spacing pitch
$\dot{q}''$	wall heat flux
r_i	inner bend radius
Re	Reynolds number
Ro	Rotation number
T, T_b, ΔT	temperature
T_P	temperature at cell adjacent to wall
T_W	temperature at wall
v, vb	mean (bulk) velocity magnitude
y^*	dimensionless wall distance
y_p	distance from point P to wall
ε	dissipation rate
κ	von Karman constant (=0.42)
μ	dynamic viscosity of the fluid
ρ	density
ω	rotational speed

INTRODUCTION

The need for cooling gas turbines has increased steadily as the difference between turbine inlet and allowable metal temperature increases. The turbine inlet temperatures for industrial and aircraft gas turbines have increased approximately 20 to 25 K per year for the past 20 years. The allowable metal temperatures have also increased but at a slower rate. In addition, the compressor pressure ratios have also increased with the result that the cooling air has higher temperatures. Continued use of the same airfoil cooling

Presented at the International Gas Turbine & Aeroengine Congress & Exhibition
Orlando, Florida — June 2–June 5, 1997

technology as the compressor discharge air temperature increases results first in no increase in power plant efficiency with increasing burner temperature. In addition to the need for using the cooling air efficiently to avoid performance penalties, the gas turbine designer is also under pressure to develop cooling configurations with a minimal number of laboratory, cascade or "rainbow wheel" tests.

Numerical modeling of the flow and heat transfer in the blade coolant passages has been long sought as an accurate, rapid and, therefore, cost-effective method of predicting local and averaged heat transfer distribution in rotating and stationary coolant passages. The current "ideal procedure" would have a designer make coolant passage geometric changes one day and have accurate numerical heat transfer results the next morning showing effects of that change on the airfoil temperature and life characteristics. Practical coolant passages include the use of heat transfer enhancing trips or ribbons at various angles to the mean flow direction in a multipass serpentine configuration and a rotating environment with rotating gravitational forces 10,000 to 40,000 times the earth's "g" force. The flow and heat transfer in these passages can be dominated by turbulent flow, the enhanced surface characteristics, the Coriolis effects or the buoyancy effects. Experimental results, showing dimensionless flow and thermal boundary conditions for all the aforementioned effects, were presented by Johnson et al. (1994).

Thus far, most of the published numerical effort has been directed toward obtaining accurate heat transfer predictions in smooth, stationary and rotating, coolant channels. Reviews of the efforts to predict heat transfer in these channels were presented by Iacovides and Launder (1995) and by Prakash and Zerkle (1992). The reader is referred to their reviews for details of previous work and to Bo et al. (1995) for a general discussion of the code algorithms and turbulence models. More recent studies, determining the effects of coolant passage aspect ratios on heat transfer in rotating passages, were conducted by Dutta et al.(1996) and Teriwal (1996).

Fewer predictions have been presented for rotating coolant passages with enhanced heat transfer surfaces with ribbons or trips. Taylor et al. (1991) showed the effects of annular ribs in a rotating cylindrical tube. A finite element method code was employed as well as "ad hoc" relationships for the turbulent Prandtl number at various values of y^+ less than 25. The calculated results were in good agreement with the experimental measurements. Abuaf and Kercher (1994) presented a numerical / experimental comparison of flow and heat transfer in a stationary large scale model of a gas turbine blade containing a three-pass serpentine passage with ribs normal to the flow direction. The computations were performed using a k-ε turbulence and a standard wall shear model. Results from the calculations were scaled to experimental conditions for the comparison. Prakash and Zerkle (1993) reviewed results from earlier exploratory calculations with ribs. In the same paper, they predicted flow and heat transfer in a ribbed rectangular duct with and without rotation, using a high Re number k- ε turbulence model with standard wall functions. Selected comparisons with correlations from the literature for stationary passages and with results from proprietary rotating experiments for rotation numbers of 0.0, 0.06 and 0.12 were satisfactory. For these calculations with ribs, the ribs were normal to the flow and buoyancy effects were neglected. As shown by Johnson et al. (1993, 1994), ribs normal to the flow can be sensitive to buoyancy effects for high rotation numbers and especially for flow inward. Consequently, important effects of buoyancy can be lost by neglecting these terms.

Although many advanced gas turbine coolant passage designs employ ribs at angles of 45 to 70 degrees to the coolant flow direction, published calculations prior to 1995 for flow in ribbed coolant passages have been for ribs normal to the flow direction and usually with buoyancy neglected. To make the calculations more relevant to current design practice, the effort of the present authors was directed toward the evaluation of calculation procedures and turbulence models with skewed rib configurations and with the inclusion of both Coriolis and buoyancy effects. These evaluations have been conducted for the experimental conditions of coolant passages with and without rotation and with smooth walls or walls with skewed trips. The comparisons were made for experimental conditions and results presented by Wagner et al. (1991) and Johnson et al. (1994) and available as NASA reports, Hajek et al.(1991) and Johnson et al. (1993). Initial results were presented by Bonhoff et al. (1996) for flow conditions without rotation and for the smooth walls and walls with 45 degree trip conditions, using FLUENT with the k-ε model, the RNG variation of the k-ε model and the Reynolds stress equations. One important conclusion from this paper was that results using the differential Reynolds stress models were consistently closer to the experimental results than those obtained using the standard or the RNG k-ε turbulence models. This was especially true for the turn region where the flow characteristics are complex and flow separation is experimentally known to occur for stationary flows and is believed to occur for rotating conditions. As a result, most of the calculations for flow conditions with rotation were performed using the differential Reynolds stress turbulence model with wall functions. This paper presents the flow characteristics and heat transfer results for the flow conditions with rotation and compares them with selected stationary results. The predicted flow characteristics show the magnitude of the secondary flows in the coolant passages and the thermal mixing mechanisms important in the prediction of local temperature and heat transfer distributions.

CONFIGURATION

The rectangular, four-pass, serpentine passage with three 180 deg. turns, that was experimentally investigated by Wagner et al. (1991) and Johnson et al. (1994), is given in Fig. 1.

This turbine blade passage geometry was chosen because a comprehensive set of heat transfer measurements was provided. Measurements were made for the stationary and rotating duct with smooth walls and with walls having normal or skewed,

staggered ribs. The duct has a rectangular cross section with a hydraulic diameter, d_H = 0.0127 m. The other geometrical dimensions are listed in Fig. 1.

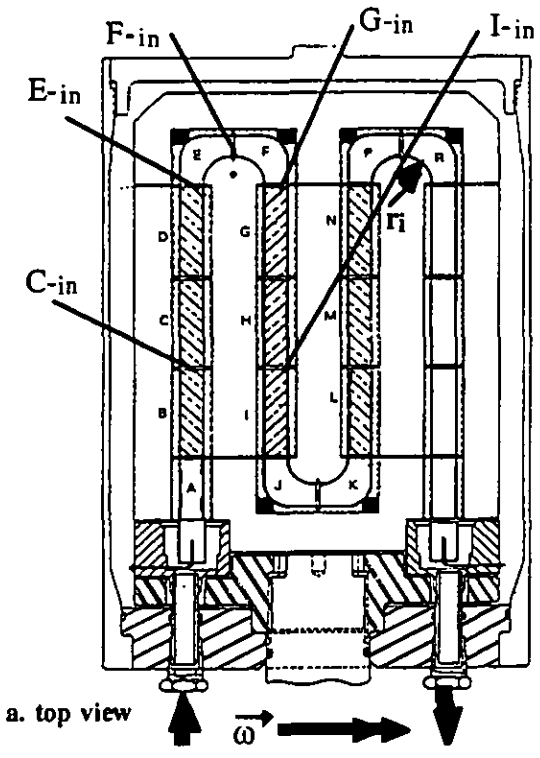

Figure 1: Cross sectional views of coolant passage heat transfer model with skewed ribs

All walls in the first three straight legs of the serpentine and the leading, trailing and the outer sidewalls in the turns are heated to a constant temperature, while the fourth leg and inner walls of all turns are covered with thermal insulation. For all sections, marked A to R in Fig. 1, constant-temperature, steady-state heat balance measurements and wall static pressure measurements were made. In the present study, the flow field and the heat transfer are simulated for the first two passages with the turn. For comparisons, the measured side-averaged Nusselt numbers for each section are used. The nomenclature A-in, B-in, .. etc. indicates the flow inlet plane for each section of the model.

ANALYTICAL MODEL

For all calculations in this study the commercial CFD-code FLUENT version 4.3 was used.

Overview

The code offers a variety of options with regard to the solution process, spatial discretization scheme and turbulence modeling. In this section, the solution process and the turbulence modeling used in this study are described briefly. For a more detailed description of the theory and the different options available, the reader is referred to Batchelor (1967) and to the FLUENT manual.

The governing equations of continuity, momentum and energy were solved using the finite volume code FLUENT version 4.3.2. This pressure-based procedure solves the full Navier-Stokes equations in general, body-fitted coordinates. A nonstaggered, control-volume storage scheme was employed where all variables were stored at the cell center. In this study, a blended second order upwind/central difference scheme was used to interpolate the values of the cell faces.

To solve the equations of continuity and momentum, the pressure-velocity coupling algorithm SIMPLE was employed. The iterative solution procedure was carried out by a Line Gauss-Seidel elimination technique. A multigrid acceleration technique was used to decrease the calculation times.

Turbulence modeling

Modeling of turbulent flows requires appropriate modeling procedures to describe the effect of turbulent fluctuations of velocity and the scalar quantities on the basic conservation equations. The conservation equations for turbulent flows were obtained from the basic equations for laminar flows using the Reynolds time averaging procedure. The resulting equations had the same form as the basic equations with the effect of turbulence incorporated through the Reynolds stress tensor.

A number of turbulence models have been developed in the last few years to model this stress tensor. The following turbulence models with a different basic approach are implemented in the used version of the code (version 4.3.2):

- k-ε model (standard)
- ReNormalisation Group (RNG) k-ε model
- Reynolds Stress model (RSM)

In a previous study by Bonhoff et al. (1996), where the same geometry was investigated without rotation, numerical results were obtained with the three turbulence models and wall functions. These results were compared with regard to their heat transfer prediction capabilities. Only the RNG k-ε model and the RSM produced adequate heat transfer results in the entrance regions. In the present study, all calculations were performed using the RSM because the currently implemented RNG k-ε model is not suitable for rotating flows. The main aspects of the implemented Reynolds stress model are briefly described below. A more detailed description of the models can be found in the FLUENT Manual, in Launder and Spalding (1972), Rodi (1984), Yakhot and Orszag (1986), Launder et al. (1975) and Launder (1989).

Reynolds Stress turbulence model. The RSM algorithm performs the calculation of the individual Reynolds stresses via differential transport equations. The transport equations are obtained from the momentum equations and contain triple-order velocity correlations and pressure-velocity correlations that must be modeled to provide closure. FLUENT's implementation of the RSM contain the model assumptions of Launder et al. (1975) and Launder (1989).

For the near-wall treatment, standard wall functions, Launder and Spalding, (1974) are used to compute the shear stresses and to set the near-wall boundary conditions for the individual stresses. The heat transfer at the walls is computed via a log-law formulation based on the analogy between heat and momentum transfer, Launder and Spalding (1974).

$$T^* \equiv \frac{(T_w - T_p)\cdot\rho\cdot c_p C_\mu^{1/4} k_p^{1/2}}{\dot{q}''} = \mathrm{Pr}_t\left[\frac{1}{\kappa}\ln\left(E\cdot y^*\right) + P\right]$$

where

$$y^* \equiv \frac{\rho C_\mu^{1/4} k_p^{1/2} y_p}{\mu}$$

and P is computed by using the formula

$$P = \frac{\pi/4}{\sin(\pi/4)}\left(\frac{A}{\kappa}\right)^{1/2}\left(\frac{\mathrm{Pr}}{\mathrm{Pr}_t} - 1\right)\left(\frac{\mathrm{Pr}_t}{\mathrm{Pr}}\right)^{1/4}$$

During the iteration, the logarithmic profile in the above equation is applied to compute the wall temperature or heat flux, depending on the type of thermal boundary condition.

The calculations are performed using the turbulence modeling constants from Launder et al. (1975). The turbulent Prandtl number was taken to be $\sigma_\theta = 0.9$.

Grid generation

Calculations were performed for the two-passage cooling channel with:

- smooth walls
- 45° angled ribs, staggered on the upper and the lower sides of the straight sections.

For the RSM with wall functions, a y^* of approximately 30 is recommended for the first cell next to a wall. Thus, a grid with 21x21 grid points in each cross section was set up.

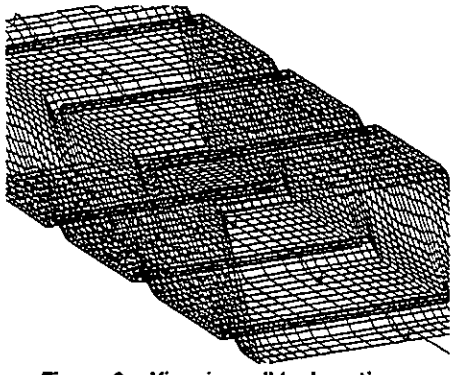

Figure 2: View in a ribbed section

For the duct with smooth walls, 220 grid lines are used in stream-wise direction with 88 lines in the first leg, 52 lines in the bend and 80 lines in the second leg. For the ribbed duct, 482 grid lines are employed in stream-wise direction with 218 lines in the first leg, 44 lines in the bend and 220 lines in the second leg. Figure 2 shows some details of the grid for the ribbed duct. To resolve the shape of the round ribs, at least 9 grid points are necessary for the approximation of each rib.

Boundary conditions

From the various experiments, those with conditions typical of modern industrial gas turbines were chosen for the present numerical investigations.

Re = 25000, $\dot{m}$ = 0.0059 kg/s, p = 10.17 bar,
T= 300.24 K, Ω = 550 rpm

Unlike the experiments, a uniform velocity profile is assumed at the inlet with a turbulence level of 3 percent. From a prestudy, it was found that this assumption influences the development of the boundary layer in the nonribbed sections of the first leg, especially section A in Fig. 1. Thus, the highest uncertainty in the calculated heat transfer data due to this assumption is expected in section A. A zero normal gradient exit boundary condition is set. The density and the properties of the fluid are taken as piecewise linear functions of the temperature.

At the wall, a uniform temperature T_w = 344.64 K, i. e. ΔT = 44.4 K is prescribed. As mentioned before, the inner surface of the bend and the heat transfer section J, Fig. 1, is unheated.

RESULTS AND DISCUSSION

In the present study, the flow and heat transfer in rotating cooling channels are investigated using CFD. Table 1 gives an overview of the calculated cases and the turbulence models that were used in the present (x) and in the previous (o) study by Bonhoff et al. (1996).

configuration/ turbulence model	stationary		rotating	
	smooth walls	ribbed walls	smooth walls	ribbed walls
standard k-ε	o	o	-	-
low-Re-RNG k-ε	o	-	-	-
RSM	o	o	x	x

o Bonhoff et al. (1996) x present study - combination not used

Table 1: Configurations and turbulence models

The main objectives of this study are:

- to compute the flow in the straight sections with and without ribs and in the bend under the influence of
  - -Coriolis force
  - -Centrifugal force / buoyancy
- to obtain a quantitative description of the local heat transfer coefficient distribution and compare with previous experiments.

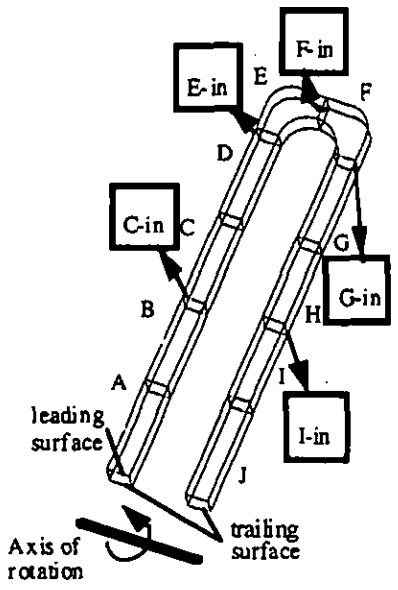

Figure 3: Geometry and axis of rotation

The computational domain is illustrated schematically in Fig. 3. It consists of one radially-outward, straight section (first leg, sections A through D in Fig. 3), one radially-inward straight section (second leg, sections G through J in Fig. 3) with the two connected by a 180 deg. bend (sections E and F in Fig. 3). These sections rotate about the axis, which is perpendicular to the straight passages, as shown in Fig. 3. In order to distinguish the four side walls of the square flow passage, the upper and lower walls, relative to the rotating direction, are called the leading and the trailing surfaces, respectively. The other two side walls are named the inner and the outer surface. In Fig. 3, the definitions of the different cross sections that are used for the discussion of the secondary flow structures are shown. In all Figures, the cross sections are viewed from an upstream position. Thus, the inner side wall is always on the right hand side.

Stationary cooling channel.

Bonhoff et al. (1996) presented numerical results of the flow and heat transfer for the same cooling channel without rotation. Some of these results are used here to discuss the effect of rotation.

Smooth walls, stationary. The calculated flow field for the smooth wall channel is presented in Fig. 4. Within the first leg of this smooth wall channel, secondary flow is produced by the nonisotropic turbulence and the developing boundary layer. The main flow (E-in in Fig. 4) is one to two orders of magnitude times this secondary flow.

Within section E, the flow is accelerated at the inner side (low pressure) and decelerated at the outer side (high pressure). This pressure gradient leads to a secondary flow in the side wall boundary layer from the outer to the inner side (Fig. 4, F-in), which forms the two counter-rotating vortices in the turn. The secondary flow starts to decrease in the second half of the turn (Fig. 4, G-in) and has almost vanished at the end of the second leg.

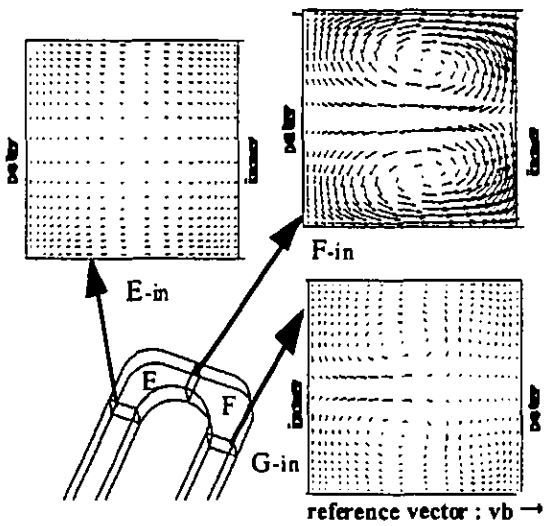

Figure 4: Secondary flow (smooth walls, stationary)

Ribbed walls, stationary. The secondary velocity vectors for the ribbed wall channel are shown in Fig. 5. In the straight sections, the flow is fully dominated by the influence of the ribs. Due to the arrangement of the ribs from the inner to the outer side in the first leg and from the outer to the inner side in the second leg, the flow is driven towards the outer side in the first straight section (Fig. 5, E-in) and towards the inner side in the second straight section (Fig. 5, I-in). As a consequence, two counter-rotating vortices are formed having different directions outboard along the endwall in the first leg and inboard along the endwall in the second leg of the channel.

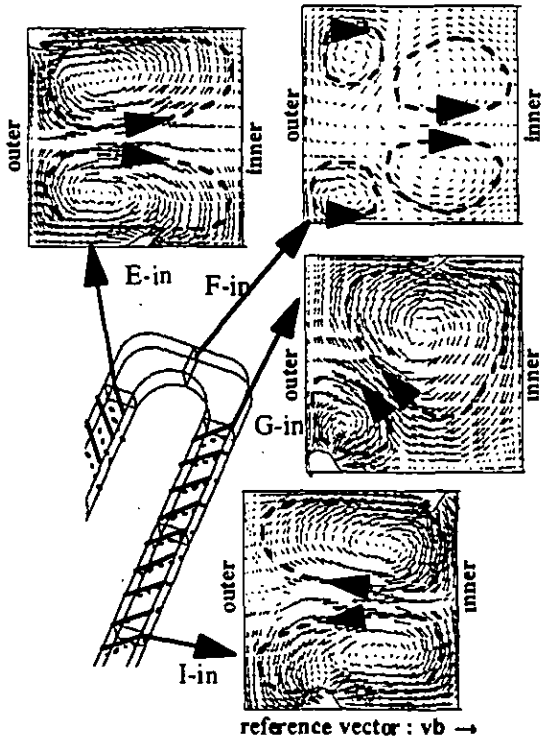

Figure 5: Secondary flow (ribbed walls, stationary)

The secondary flow in the turn is shown in Fig. 5, F-in. The two counter-rotating vortices from the first leg are entering the turn. The orientation of the flow in these vortices on the sidewalls is towards the outer side. Within the turn, the same effects, discussed above for the smooth-wall channel, lead to two additional vortices that are contrary to the orientation of the incoming vortices (Fig. 5, E-in). At the end of the turn, only the curvature-induced vortices remain (Fig. 5, G-in). The two pairs of vortices (F-in) have counter effects; thus, the secondary flow in the turn is reduced for the stationary ribbed wall case.

Rotating cooling channel

For flow in rotating radial coolant passages, the following two additional forces are acting on the flow:

Coriolis force: $f_{CO} = 2 \cdot \rho \cdot \omega \times v$

Centrifugal force: $f_{CE} = \rho \cdot \omega \times (\omega \times r)$

Figure 6 illustrates the secondary flow patterns that are induced in the rotating flow passages, both when the fluid is flowing outward from and inward toward the axis of rotation.

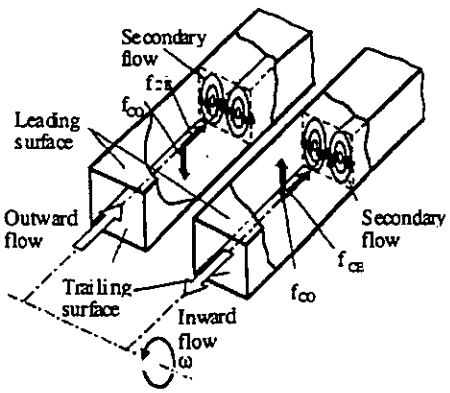

Figure 6: Generation of secondary flows in the outward and inward sections due to rotation, Mochizuki et al. (1994)

When a fluid flows in a tube rotating about an axis that is perpendicular to the tube axis, a centrifugal force acts on every part of the fluid. In the case of heated flows, centrifugal buoyancy forces become an important factor. Relative to the mean flow, centrifugal buoyancy forces accelerate the cold, more dense fluid particle away from the center of rotation, while the hot and lighter fluid along the heated walls tends toward the center of rotation. In the first straight section of the model (Fig. 6), the light fluid motion opposes that of the mainstream flow. In the second model passage, where the coolant flows toward the axis of rotation, the mainstream and buoyancy force directions become aligned.

The Coriolis force, whose magnitude is proportional to the radial component of the flow velocity, acts in the direction perpendicular to axis of the channel. The direction of the Coriolis force varies with the direction of the main flow (outward or inward), as shown in Fig. 6. Due to the viscous effects, the velocity is smaller near the channel walls and larger near the axis of the channel. Thus, a relatively larger Coriolis force appears in the center, and consequently a secondary flow is produced, as shown schematically in Fig. 6. The rotational directions of these secondary vortices are opposite to those of the main outward and inward flows.

Smooth walls, rotating. The calculated flow field for the rotating smooth wall channel is presented in Figs. 7 and 8. The left side in Fig. 7 shows the lines of constant velocities at the entrance of the different sections, as defined in Fig. 3. Note that the scale of the velocity vectors is magnified by 5 times in Fig. 7 for C-in and I-in. In the middle of the outward leg (C-in, Fig. 7), the Coriolis-induced secondary flow is clearly shown by the two large counter-rotating vortices. The cold fluid from the middle of the channel is transported towards the trailing surface where it turns twice and flows back to the leading surface along the side walls. At the side walls, the fluid is heated and the buoyancy effects are growing.

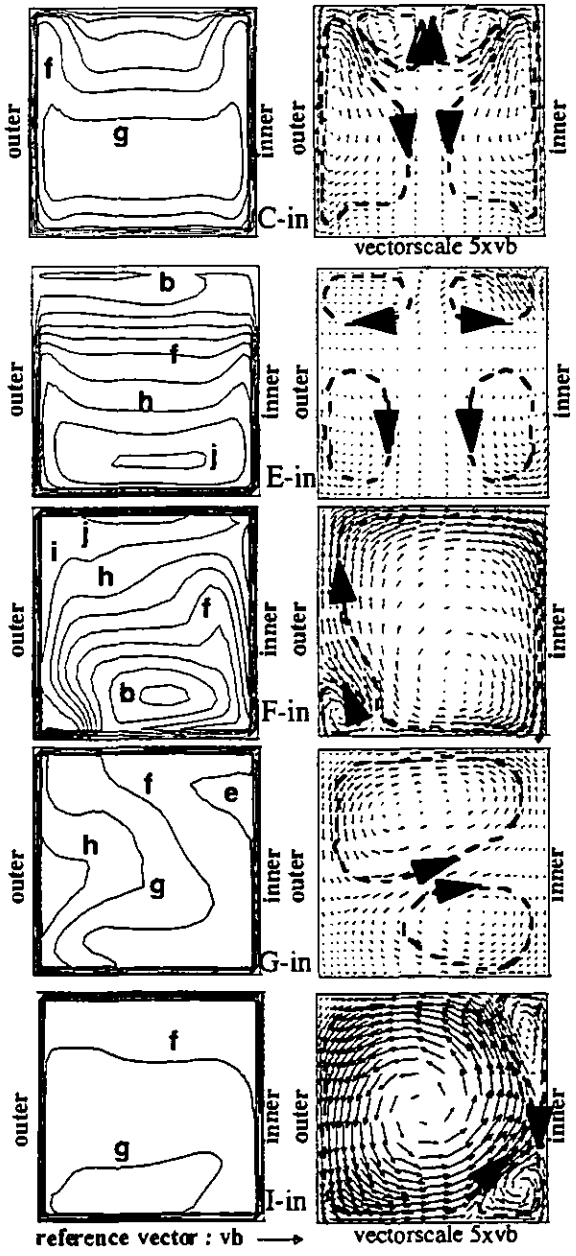

labels (v/vb): e=0.8; f=1.0 g=1.2; h=1.4

Figure 7. Contours of constant velocities and secondary flow (smooth walls, rotating)

Two additional smaller counter-rotating vortices are formed at the leading surface. These vortices were also found by Bo et al. (1995) in a numerical study for nonbuoyant flow in a one-passage cooling channel with the same rotation and Reynolds number. The fluid is transported towards the trailing surface, the main flow velocity increases near the trailing surface and decreases near the leading surface. This leads to a further increased Coriolis force at the trailing surface and an increased buoyancy effect at the leading surface. At the end of the first leg (Fig. 7, E-in), reversed flow appears in a region up to approximately 20 percent of the channel height near the leading surface in Fig. 8.

In the turn, the Coriolis forces decrease rapidly with the change of direction of the main flow. Also, the secondary flow from the outer to inner wall that was observed in the stationary case, starts to recover due to the pressure gradient. The Coriolis force-induced vortex on the inner side wall and the pressure-induced vortex on the trailing surface have different orientations, while the incoming vortex on the outer side and the pressure-induced vortex at the leading surface have the same orientation. Consequently, the outer side and leading surface vortices combine into one large vortex. From the other two vortices, only that induced by the pressure gradient is visible in a small region on the outer wall in Fig. 7, F-in. The highest velocity, which can be found near the trailing surface at the entrance of the turn, is shifted to the leading surface in the middle of the turn.

In the second leg, where the mainstream and buoyancy force directions are aligned, only the Coriolis force-induced secondary flow is visible at the entrance of section 1 (Fig. 7, I-in).

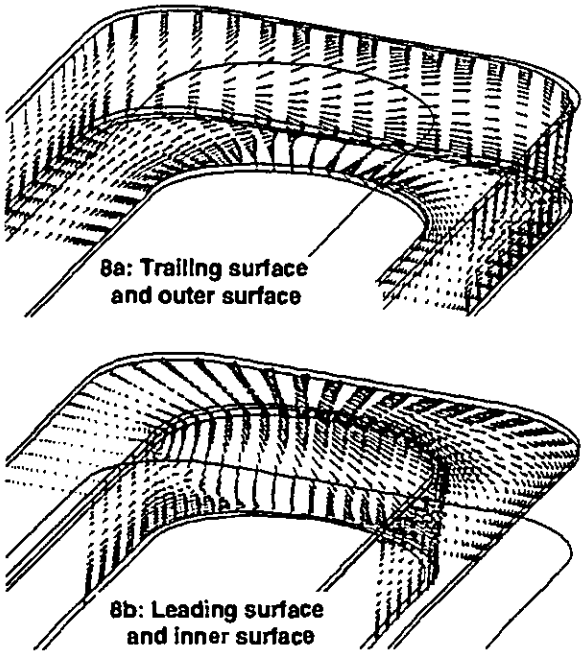

Figure 8. Velocity vectors at planes 5 percent d_H from the wall (smooth walls, rotating)

In Fig. 9, the calculated lines of constant heat flux are shown on the leading and trailing surface. The highest heat flux arises at the beginning of section A, the first heated section.

Within sections A and B on the trailing surface, the heat flux decreases slowly in the streamwise direction and, due to the accelerating flow, the heat flux increases again in sections C and D, reaching its maximum value at the entrance of the turn. On the leading surface, the heat flux decreases much more steeply in the streamwise direction. It reaches its minimum in section C (elliptic line of constant heat flux in Fig. 9). This is the area where the flow changes direction. Due to the high velocities in the flow direction from the trailing surface at the beginning of the turn to the leading surface in the middle of the turn, the heat flux increases on the leading surface and decreases on the trailing surface. In the second leg, the heat flux is very similar on both surfaces. With the inverted Coriolis force and the resulting secondary flow, it is slightly higher on the leading surface.

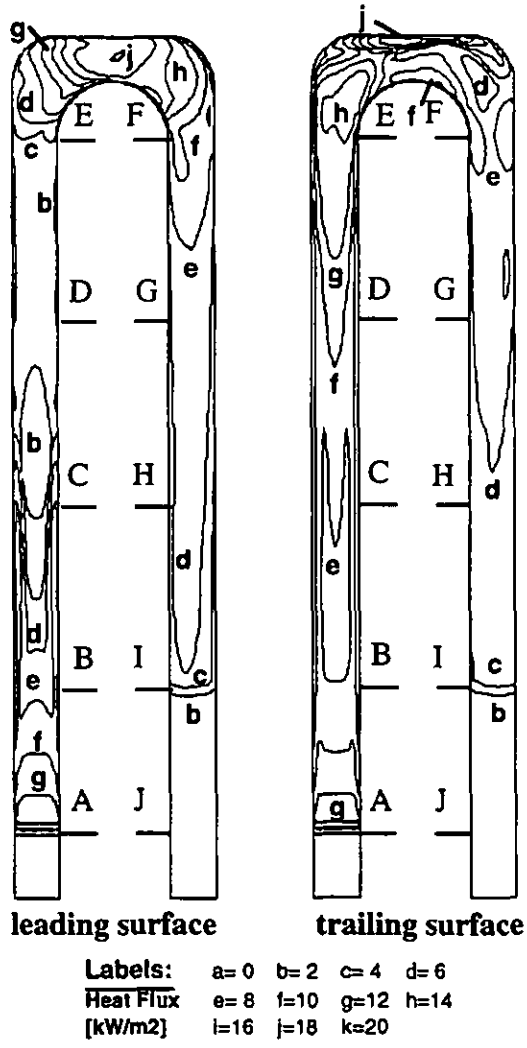

Figure 9. Contours of constant heat flux (smooth walls, rotating)

The segment-averaged Nusselt numbers on all four walls are shown in Fig. 10. The segment-averaged Nusselt number was computed for all heat transfer sections using the local mass-averaged temperature, T_b, in each section. The transport properties were related to the average of the bulk and the wall temperature. The Nusselt numbers that were used for the comparison between measurements and calculations are the side-averaged Nusselt numbers divided by the Nusselt number for a fully-developed flow in a square duct Nu_∞, with the same hydraulic diameter and the same Reynolds number at the inlet. The constant heat flux Colburn equation, adjusted for constant wall temperature, was used to obtain the Nusselt number for fully developed, turbulent flow in a smooth duct, Kays and Perkins, (1973). The resulting equation for the constant wall temperature condition with a Prandtl number equal to 0.72 is as follows:

$$Nu_\infty = 0.0176 \cdot Re^{0.8}$$

The experimental data and the numerical results for the rotating and nonrotating smooth walls cooling channel are plotted in Fig. 10. The main effects, previously discussed for the local numerical heat transfer results in Fig. 9, can also be found in the experimental data. On the leading surface, the Nusselt number decreases to approximately half that of the nonrotating channel. In the turn (Sections E and F), the Nusselt numbers increase very rapidly to about 3.0*Nu∞, which is 4 to 5 times greater than those in section D.

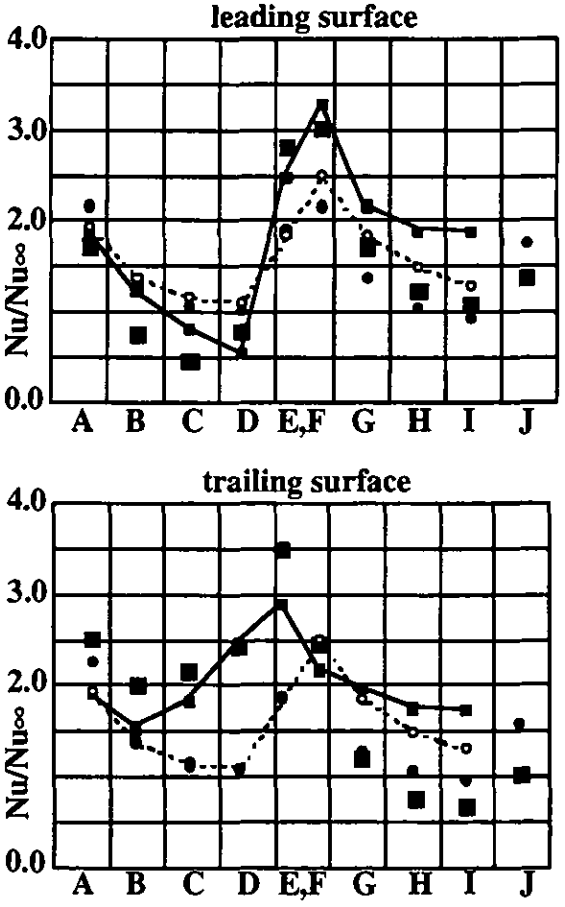

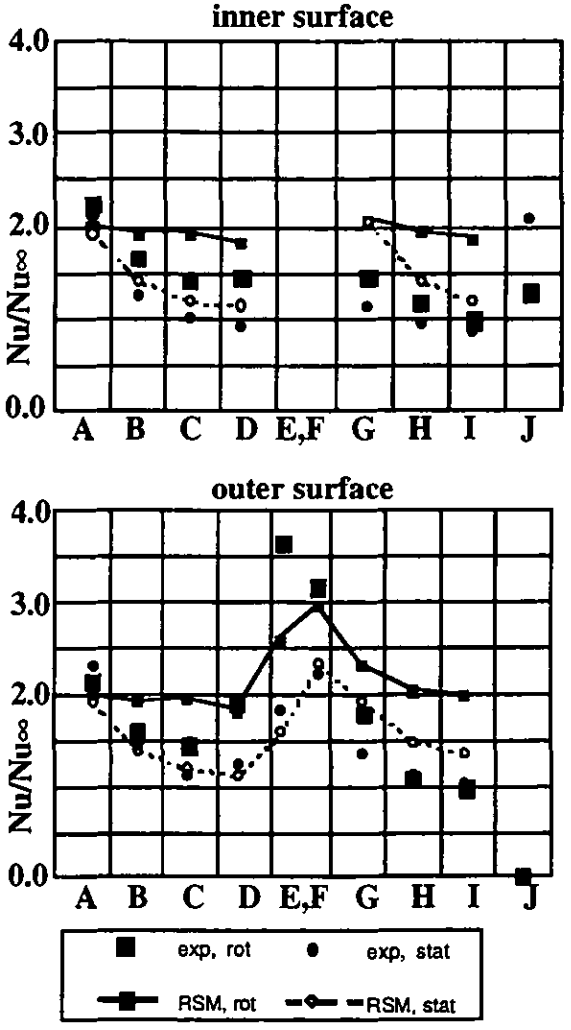

Figure 10. Comparison of experimental and numerical segment-averaged Nusselt number distribution (smooth walls, rotating and stationary)

On the trailing surface, the heat transfer decreases from section A to section B and increases again to about 2.5 times the Nusselt number for the nonrotating case. The heat transfer on the inner and outer surface is, in general, slightly higher for the rotating channel. The biggest differences are in the turn at the outer surface where the Nusselt number is about twice as high with rotation, compared to the stationary flow conditions.

In the second leg, the experimental Nusselt numbers decrease on all walls to about 1*Nu∞ in section I. The comparison between the experimental data and the predictions shows that the differences are high compared to the stationary case. Although the Nusselt number magnitude differs in some sections between the measurements and predictions, e. g. in the turn on the trailing and outer surface, the principle effects of rotation are predicted in the first leg and in the turn.

The overpredictions of the Nusselt numbers in the second leg, also found in the stationary cases, are greater with rotation.

Ribbed walls, rotating. The calculated velocity contours and the secondary flow field for the rotating ribbed wall channel are presented in Figures 11 and 12. The structure of the secondary flow, which is almost fully developed after section B (the first section with ribs; see Fig. 11,C-in), can easily be interpreted as a combination of the secondary flow in a ribbed, stationary channel (Fig. 5) and the secondary flow in a rotating smooth channel (Fig. 7).

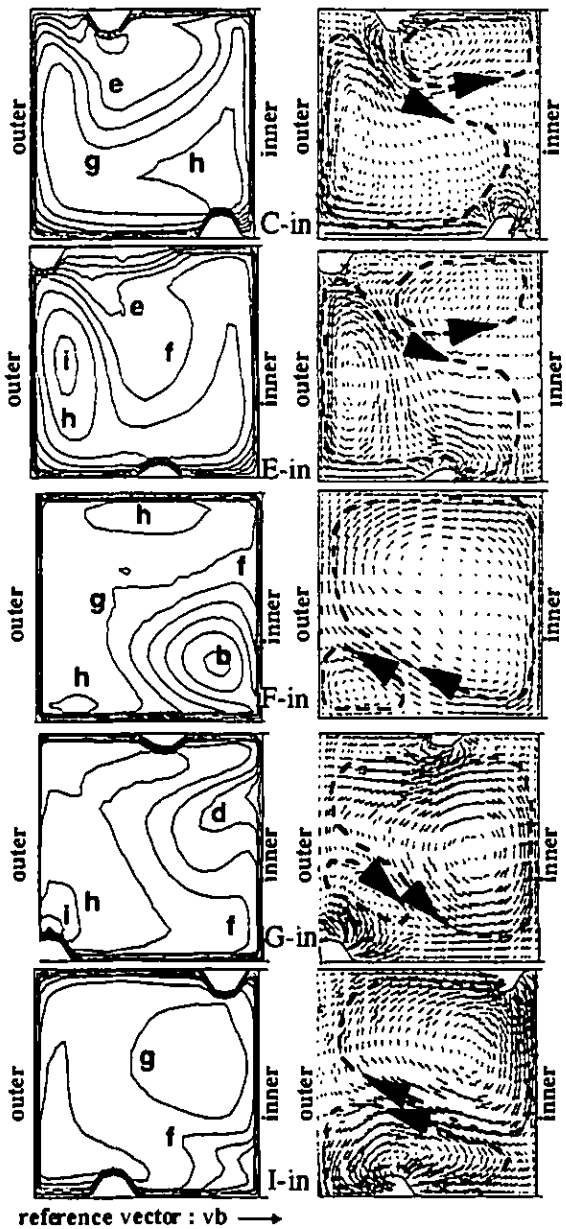

Figure 11. Contours of constant velocities and secondary flow (ribbed walls, rotating)

In the second leg, where the orientation of the ribs and the orientation of the Coriolis force have changed, the same flow structure can be found but with reversed signs (Fig. 11, I-in). In the nonribbed turn, the secondary flow structure is very similar to that of the rotating smooth wall case (Fig. 11, F-in and Fig. 12).

From the ribbed wall case, the vortex from the inner to outer side wall combines with the Coriolis-induced vortex of the rotating smooth wall case from the trailing to the leading surface. Both vortices have the same orientation. Therefore, one large diagonal vortex is formed. In a similar way, a corresponding counter-rotating vortex is formed in the opposite corner but with a smaller secondary flow magnitude.

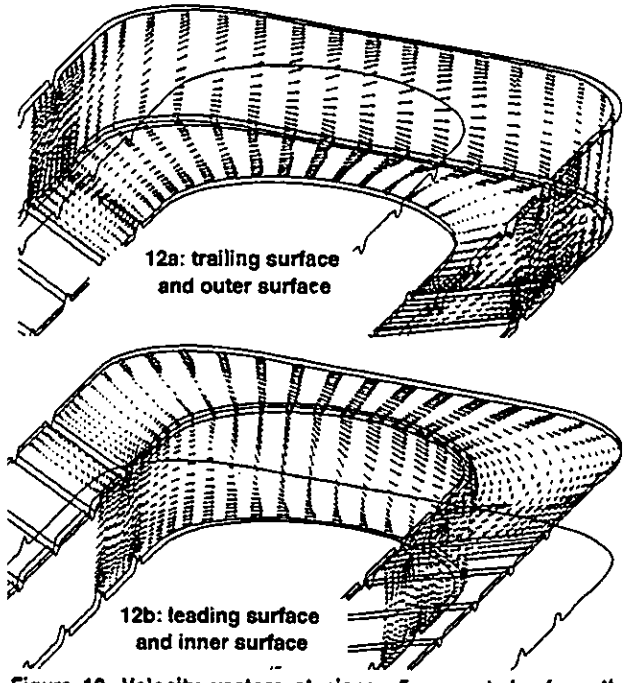

Figure 12. Velocity vectors at planes 5 percent d_H from the wall (ribbed walls, rotating)

Compared to the rotating smooth wall channel, the ribs lead to the following important changes in the flow field:

- more mass is being transported to the leading surface and therefore no reversed flow zone exists
- the velocities are lower in the ribbed channel
- the magnitude of the secondary flow in the turn is lower

The calculated lines of constant heat flux for the rotating ribbed model are shown in Fig. 13. Although the structure of the isolines in the straight sections is somewhat irregular, the patterns are similar between the ribs.

The peak heat flux in the first leg on the leading surface decreases from section to section, while it stays at approximately the same level on the trailing surface. Between two ribs on the leading surface, the heat flux is decreasing significantly from the middle towards the outer side in a region of approximately 20 percent of the surface area. A similar behavior can be seen in the second leg of the opposite surfaces. In the turn, the heat flux is slightly less than in the rotating smooth-wall channel.

The heat fluxes in the developed flow region of the second leg will be lower than in the developed flow region of the first

leg due to increasing bulk temperature for this constant wall temperature condition.

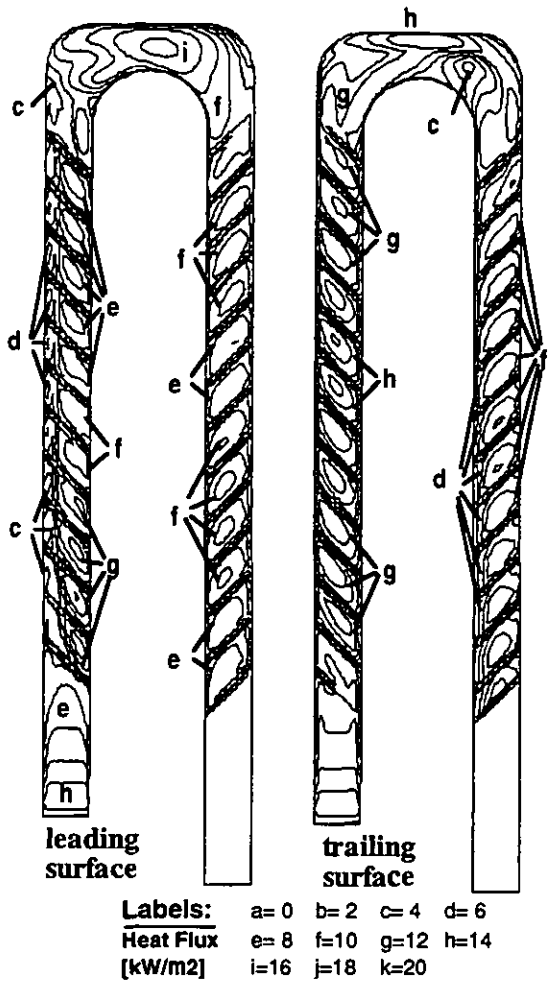

Figure 13. Contours of constant heat flux (ribbed walls, rotating)

The measured and the calculated section-averaged Nusselt numbers for all sections at the different walls are shown in Fig. 14. For comparison, the results for the stationary, ribbed-wall channel (circles) and the rotating, smooth-wall channel (triangles, only at leading and trailing surfaces) are plotted with light gray symbols.

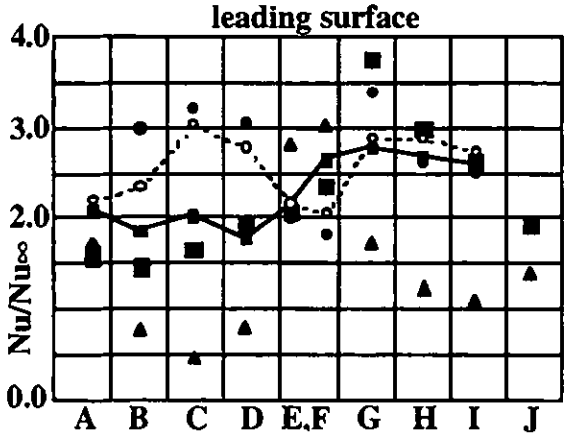

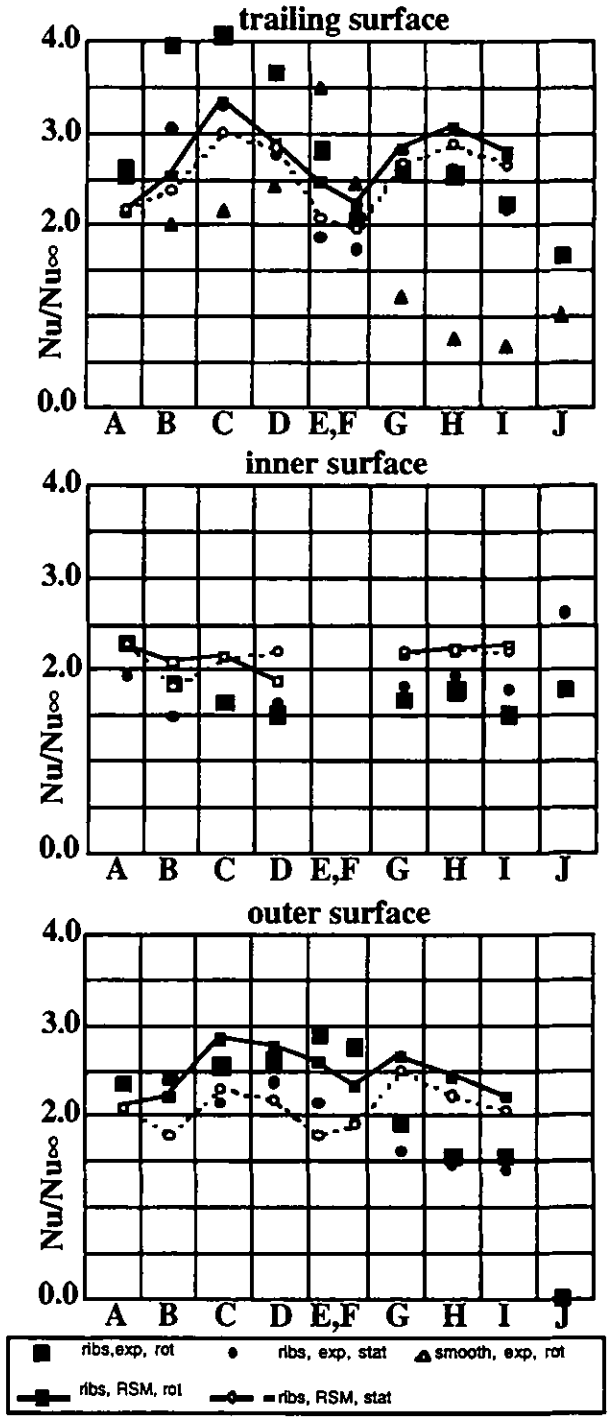

Figure 14. Comparison of experimental and numerical segment-averaged Nusselt number distribution (ribbed walls, rotating and stationary)

In the first leg of the model, the predicted decreases and increases in the heat transfer coefficients on the leading and trailing surfaces, respectively, are somewhat less than measured. For the leading surface of section C, the measured heat transfer coefficient with rotation is decreased approximately 45 percent compared to the stationary and the predicted heat transfer coefficient with rotation is decreased

approximately 33 percent compared to the stationary. For the trailing surface of same section, the measured heat transfer coefficient with rotation is increased approximately 35 percent compared to the stationary and the predicted heat transfer coefficient with rotation is increased only 10 percent compared to the stationary. Thus, the predicted trends are correct but the magnitude of the changes are less than measured.

In the second leg, relatively small effects of rotation are predicted, i.e., increases and decreases in the heat transfer coefficients of 10 percent on the leading and trailing sides of section H, respectively. The measured increases and decreases were 15 and 0 percent, respectively. The high heat transfer coefficient measured on the leading surface of Section G was not predicted for either the rotating or stationary flow condition. Explanations for this anomalous measurement were not presented by the experimenters.

The predicted average heat transfer coefficients on both legs of the inner surface are 10 to 20 percent greater than measured. The predicted average heat transfer coefficients on the outer surface are 10 to 20 percent different than those measured in the first leg and approximately 25 percent lower than those measured in the second leg.

Wagner et al. (1991) and Johnson et al. (1994) noted that the heat transfer characteristics in the second leg with flow radially inward were different than those in the first and third leg with flow radially outward. One explanation is that the turbulent structure for the inward-flowing leg is different than that for the outward-flowing legs due to free convection velocities near the wall aiding or opposing the forced convection flow. Additional experiments and/or analytical modeling will be required to resolve this hypothesis.

SUMMARY OF RESULTS

A numerical study of the flow and heat transfer in rotating U-shaped cooling channels with smooth wall and with skewed ribs was performed using the FLUENT code. Comparisons from a previous study with stationary cooling channels were used to show and explain the effects of rotation. The comparison between previous measurements and the numerical results was used to determine the accuracy of the numerical predictions for heat transfer calculations.

The main findings of the study may be summarized as follows.

a) Numerical results show that strong secondary flow is produced by pressure gradients, rotational effects and the ribs:
   - in the turn, two counter-rotating vortices are formed, induced by the pressure gradient between the inner and outer surface. The orientation of the vortices on the sidewalls is towards the inner wall.
   - the Coriolis force induces secondary flow in the straight sections; in the outward leg from the leading to the trailing surface, and in the inward leg from the leading to the trailing surface, respectively.
   - the centrifugal buoyancy accelerates the flow at the leading surface in the outward leg opposite to the main flow direction. In the inward leg at the trailing surface, the buoyancy force and the main flow direction are aligned.
   - in the ribbed sections, two vortices are generated. With the given orientation of the ribs, the flow is driven towards the outer side in the first leg and towards the inner side in the second leg, respectively.

These effects are generally predicted by the numerical procedure. Depending on the case, the resulting secondary flow structure is a combination of the above-mentioned effects where some secondary flow effects are decreasing while others are increasing.

b) Rotation has an impact on the local and averaged heat transfer:
   - in the outward leg, the heat transfer changes significantly due to rotation. The heat transfer increases at the trailing surface and decreases at the leading surface.
   - in the inward leg, the changes are minor for the smooth wall case and almost negligible for the ribbed wall case.
   - on the inner and outer surfaces, the heat transfer is increased with rotation.

Heat transfer characteristics and trends resulting from these flows are in general agreement with previous experimental results.

c) The agreement of the heat transfer predictions with the experimental results depends strongly on the complexity of the secondary flow:
   - the major influence of rotation is predicted.
   - with rotating smooth walls, the agreement between the predicted heat transfer and the measurements in the first leg is good. However, the predicted heat transfer coefficients in the second leg are up to two times greater than those measured.
   - with the rotating ribbed side walls, all major variations in the heat transfer distribution were predicted correctly, although the predicted heat transfer on the leading surface was lower than the experimental measurement.

The results from the present study show that the numerical predictions provide characteristics of the flow field, which lead to a better understanding of the physics and turbulent transport mechanisms in the cooling channels of turbine blades. Further study is required to separate Corilois and centrifugal buoyancy effects by choosing different wall-to-fluid flow temperatures. At this stage, numerical predictions can be used as a cost-effective design tool to predict cause-effect relationships, although the differences between experimentally and numerically determined heat transfer distributions are greater than desired.

ACKNOWLEDGMENTS

This study was supported by ABB as part of a Corporate Research project and as a Diploma thesis for Uwe Tomm, RWTH Aachen.

REFERENCES

Abuaf, N and Kercher, D. M., 1994, "Heat Transfer and Turbulence in a Turbulated Blade Cooling Circuit", ASME Journal of Turbomachinery, Vol. 116, pp. 169-177.

Batchelor, G.K., 1967, "An Intrnduction to Fluid Dynamics", Cambridge Univ. Press, Cambridge, UK

Bo, T., Iacnvides, H, and Launder, B. E., 1995, "Convective Discretization Schemes for the Turbulence Transport Equaiions in Flow Predictions Through Sharp U-Bends", 1995, Int. J. of Num. Methods. fnr Heat & Fluid Flow, Vol. 5, pp. 33-48.

Bo, T., Iacovides, H. and Launder, B.E., 1995, "Developing Buoyancy-Modified Turbulent Flow in Ducts Rntating in Orthogonal Mode", ASME, Jnurnal of Turbomachinery, Vol. 117, pp. 474-484

Bonhoff, B., Tomm, U., Johnsnn, B. V., 1996, "Heat Transfer Predictions for U-Shaped Cnnlant Channels with Skewed Ribs and with Smooth Walls", ASME 96-TA-007, ASME Turbo Asia, Jakarta, Indonesia

Dutta, S, Andrews, M. J. ,and Han,J-C., 1996, Prediction of Turbulent Flow and Heat Transfer in Rotating Square and Rectangular Smooth Channels, ASME Preprint 96-GT-234

FLUENT User's Guide, 1995, Version 4.3, Vol. I-IV, Fluent Deutschland GmbH.

Hajek, T. J. Wagner, J. H, Johnson, B. V., Higgens, A. W., and Stueber, G. D.,1991, "Effects of Rotation on Coolant Passage Heat Transfer: Volume I-Conlant Passages with Smooth Walls", NASA Contractors Report 4396, Vol. I.

Iacovadies, H. and Launder, B. E., 1995, "Computational Fluid Dynamics Applied to Internal Gas-Turbine Conling: A Review", Inter. J. Heat and Fluid Flow, Vol.. 16, pp. 454-470.

Johnson, B. V., Wagner, J. H., and Stueber, G. D., 1993, "Effects of Rotation on Coolant Passage Heat Transfer: Volume II-Coolant Passages with Trips Normal and Skew to the Flow", NASA Contractors Report 4396, Vol. II.

Johnson, B. V., Wagner, J. H., Steuber, G. D., and Yeh, F. C., 1994, "Heat Transfer in Rotating Serpentine Passages with Trips Skewed to the Flow", ASME Journal of Turbomachinery, Vol. 116, pp. 113-123.

Kays, W. M., Perkins, H. C., 1973, "Forced Convection, Internal Flow in Ducts", from Handbook of Heat Transfer Rohsenow, W. M. and Hartnett, J. P., McGraw Hill, pp. 7-28 and 7-33.

Launder, B. E., 1989, "Second-Moment Closure: Present ... and Future?", Inter. J. Heat Fluid Flow, Vol. 10, No. 4, pp. 282-300.

Launder, B. E., Reece, G. J., and Rodi, W., 1975, "Progress in the Development of a Reynolds Stress Turbulence Closure", J. Fluid Mech., Vnl. 68(part 3), pp. 537-566.

Launder, B. E. and Spalding, D. R., 1972, "Lectures in Mathematical Models of Turbulence", 1972, Academic Press, London, England.

Launder, B. E. and Spalding, D. R., 1974, "The Numerical Computation of Turbulent Flows", Computer Methods in Applied Mechanics and Engineering, V. 3, pp. 269-289

Prakash, C., and Zerkle, R.,1992, "Prediction of Turbulent Flow and Heat Transfer in a Radial Rotating Square Duct", ASME Journal of Turbnmachinery, Vol. 114, pp. 835-846.

Mochizuki, S., Takamura, J., Yamawaki, S., Yang, Wen-Jei, 1994, "Heat Transfer in Serpentine Flow Passages With Rotation", ASME, Journal of Turbomachinery, Vol. 116, pp. 133-140

Prakash, C., and Zerkle, R.,1993, "Prediction of Turbulent Flow and Heat Transfer in a Ribbed Rectangular Duct with and without Rotation", ASME preprint 93-GT-206.

Rodi, W., 1984, "Turbulence Models and their Application in Hydraulics", Delft, The Netherlands, IAHR.

Taylor, C., Xia, J. Y., Medwell, J. O., and Mnrris, W. D., 1991, "Numerical Simulation nf Three Dimensional Turbulent Flow and Heat Transfer within a Multi-Ribbed Cylindrical Duct", ASME Preprint 91-GT-8.

Tekriwal, P., 1996, Effect of Aspect Ratio on the Buoyancy Driven Reverse Flow Near the Leading Wall of Rotating Coolant Passages", ASME Preprint 96-GT-173.

Wagner, J. H, Johnsnn, B. V., and F. C. Kopper, 1991, "Heat Transfer in Rotating Serpentine Passages With Smnoth Walls", ASME Journal of Turbomachinery, Vol. 113, pp. 321-330.

Yakhot, V., Orszag, S. A., 1986, "Renormalisation Group Analysis of Turbulence", I. Basic Theory, Journal of Sci. Comput., Vol. 1, No. 1, pp. 1-51.